

Supplement of Atmos. Chem. Phys., 19, 8471–8490, 2019
<https://doi.org/10.5194/acp-19-8471-2019-supplement>
© Author(s) 2019. This work is distributed under
the Creative Commons Attribution 4.0 License.



Supplement of

Impact of particle number and mass size distributions of major chemical components on particle mass scattering efficiency in urban Guangzhou in southern China

Jun Tao et al.

Correspondence to: Leiming Zhang (leiming.zhang@canada.ca) and Jun Tao (taojun@scies.org)

The copyright of individual parts of the supplement might differ from the CC BY 4.0 License.

Contents:

Section S1. Description of the procedure generating the continuous mass size distribution

Table S1. The refractive indices and densities of chemical species.

Figure S1. The estimated particle losses in different sizes from the tube.

Figure S2. Correlations between particle and their chemical compositions by the size-segregated samples and those by the PM₁₀/PM_{2.5} samples.

Figure S3. Single particle scattering efficiencies of the dominant chemical species.

Figure S4. Continuous log-normal size distributions of seasonal average densities in four seasons.

Figure S5. Continuous log-normal size distributions of K⁺ in four seasons.

Figure S6. Correlations between Ca²⁺ and fine soil concentrations (2.20[Al]+2.49[Si]+1.63[Ca]+2.42[Fe]+1.94[Ti]) in four seasons in Guangzhou during 2014.

Figure S7. Correlations between filter-base and online NO₃⁻ concentrations in four seasons in Guangzhou.

Figure S8. Correlations between the measured b_{sp} (<100 μm) at wavelength of 520 nm under dry condition (relative humidity <30%) and estimated b_{sp} (<10 μm) using average MSEs of chemical species at wavelength of 550 nm under dry condition (relative humidity =40%) in four seasons.

Section S1. Description of the procedure generating the continuous mass size distribution

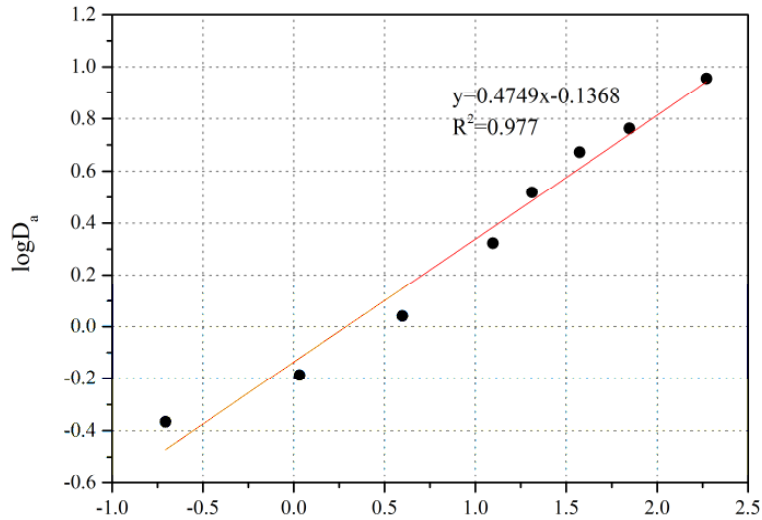
The total (PM₁₀) mass concentration is first obtained by summing those from every stage of Anderson cascade sampler. In the example shown below, concentration at the nine stages were 1.04, 1.18, 0.92, 0.60, 0.18, 0.16, 0.11, 0.09, and 0.05, respectively, and the total mass concentration was 4.33 $\mu\text{g m}^{-3}$.

Stage	Size Range	Mass	D _a (μm)	Cumulative mass <D _a	Cumulative % <D _a
0	9.0-10 μm	0.05	10	4.33	100.00%
1	5.8-9.0 μm	0.09	9	4.28	98.9%
2	4.7-5.8 μm	0.11	5.8	4.19	96.8%
3	3.3-4.7 μm	0.16	4.7	4.08	94.2%
4	2.1-3.3 μm	0.18	3.3	3.92	90.5%
5	1.1-2.1 μm	0.60	2.1	3.74	86.4%
6	0.65-1.1 μm	0.92	1.1	3.14	72.5%
7	0.43-0.65 μm	1.18	0.65	2.22	51.3%
F	<0.43 μm	1.04	0.43	1.04	24.0%

The cumulative mass of particles smaller than 0.43 μm was 1.04 $\mu\text{g m}^{-3}$, or 24.0% of the total, and that of particles smaller <1.1 μm was 3.14 $\mu\text{g m}^{-3}$, or 72.5% of the total. Assuming a log-normal particle size distribution, the cumulative percentage of particles with sizes less than a given diameter is considered as the probability of the log-normal size distribution. Thus, we plot the cumulative percentage of particle with size less than each given diameter in the log-probability coordinate system with D_a as the ordinate and the cumulative percent less than D_a as the abscissa.

For a log-normal particle size distribution, the mass mean aerodynamic diameter (MMAD) corresponds to the 50% cumulative percentage (here marked as 50% diameter), and the particle size geometric standard deviation (σ) is given by: $\sigma = (84.13\% \text{ diameter} / 15.87\% \text{ diameter})^{1/2}$, where 84.13% diameter and 15.87% diameter correspond to the diameters of the 84.13% and 15.87% cumulative probability, respectively.

For simple calculation, we use the coordinate system with logD_a as the ordinate and the inversion of cumulative percentage less than D_a of a standard normal distribution as the abscissa to represent the log-probability coordinate system mentioned above. The inversion value of the cumulative percentage can be calculated using the 'NORM.S.INV' function in the Microsoft Excel. For a log-normal distribution, the logD_a values linearly correlate with the inversion values as shown in the figure below.



Inversion of the cumulative probability of the standard normal distribution

For the standard normal size distribution, the inversion value of zero corresponds to the 50% cumulative probability of the distribution. Thus, the y-intercept of the linear regression of $\log D_a$ against the inversion (i.e., -0.1368 in this example) represents the 50% diameter, i.e., the $\log(\text{MMAD})$. The inversion values 1 and -1 correspond to the 84.13% and 15.87% cumulative probability, respectively, of the size distribution. Thus, the $\log \sigma$ can be calculate as the slope value (i.e., 0.4749 in this example) of the linear regression. As a result, the MMAD and σ of the log-normal distribution can be estimated as 0.73 and 2.98 μm in this example.

Table S1. The refractive indices and densities of chemical species.

Chemical species	refractive index	density (g cm ⁻³)	Chemical species	refractive index	density (g cm ⁻³)
NaCl	1.54-0i	2.16	Ca(NO ₃) ₂	1.53-0i	2.50
NaNO ₃	1.59-0i	2.26	H ₂ O	1.33-0i	1.00
Na ₂ SO ₄	1.48-0i	2.68	OM	1.55-0i	1.40
(NH ₄) ₂ SO ₄	1.53-0i	1.76	EC	1.80-0.54i	1.50
NH ₄ NO ₃	1.55-0i	1.73	crystal element oxides	1.56-0.01i	2.66
K ₂ SO ₄	1.49-0i	2.66	unidentified fraction	1.58-0.01i	2.00
CaSO ₄	1.57-0i	2.61			

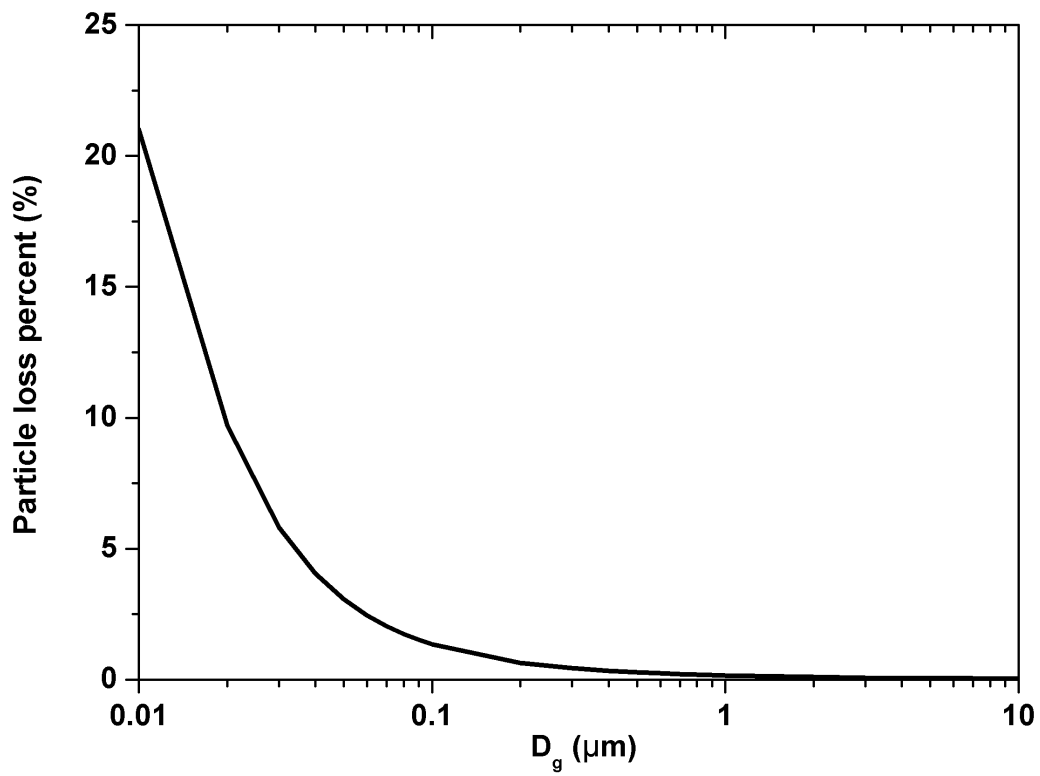


Figure S1. The estimated particle losses in different sizes from the tube.

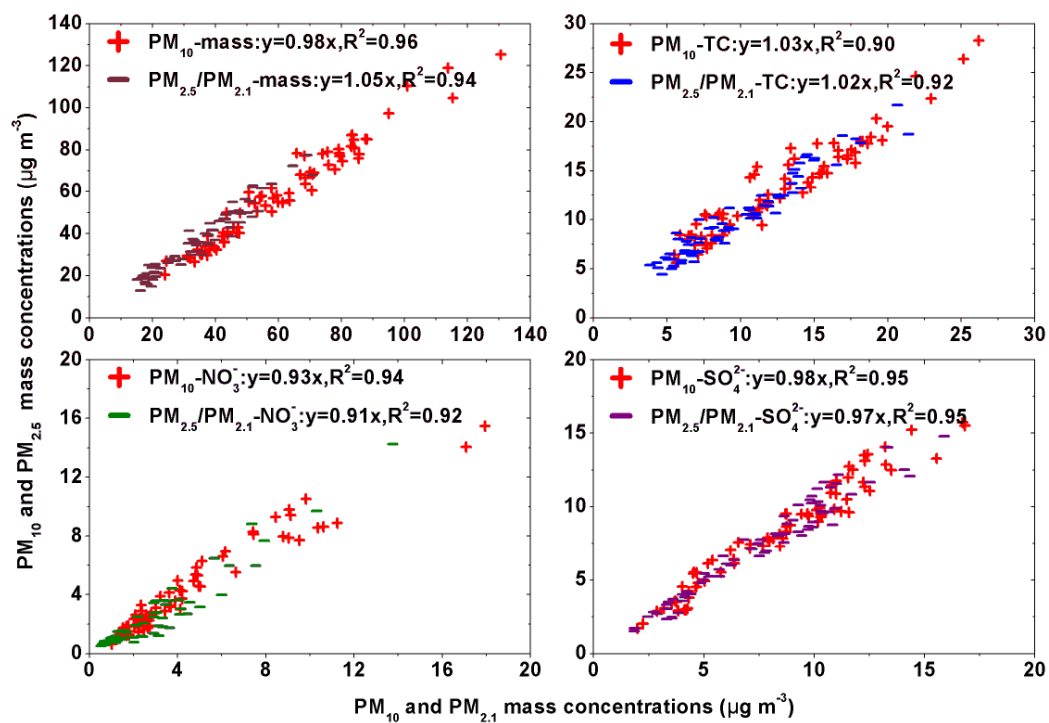


Figure S2. Correlations between particle and their chemical compositions by the size-segregated samples and those by the PM₁₀/PM_{2.5} samples.

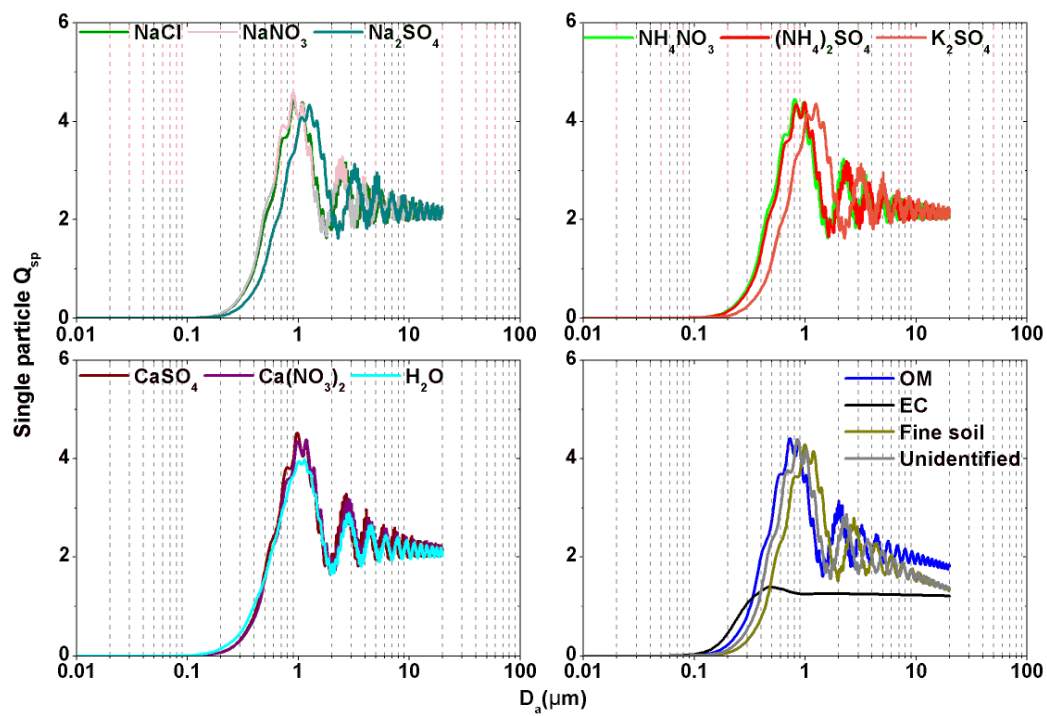


Figure S3. Single particle scattering efficiencies of the dominant chemical species.

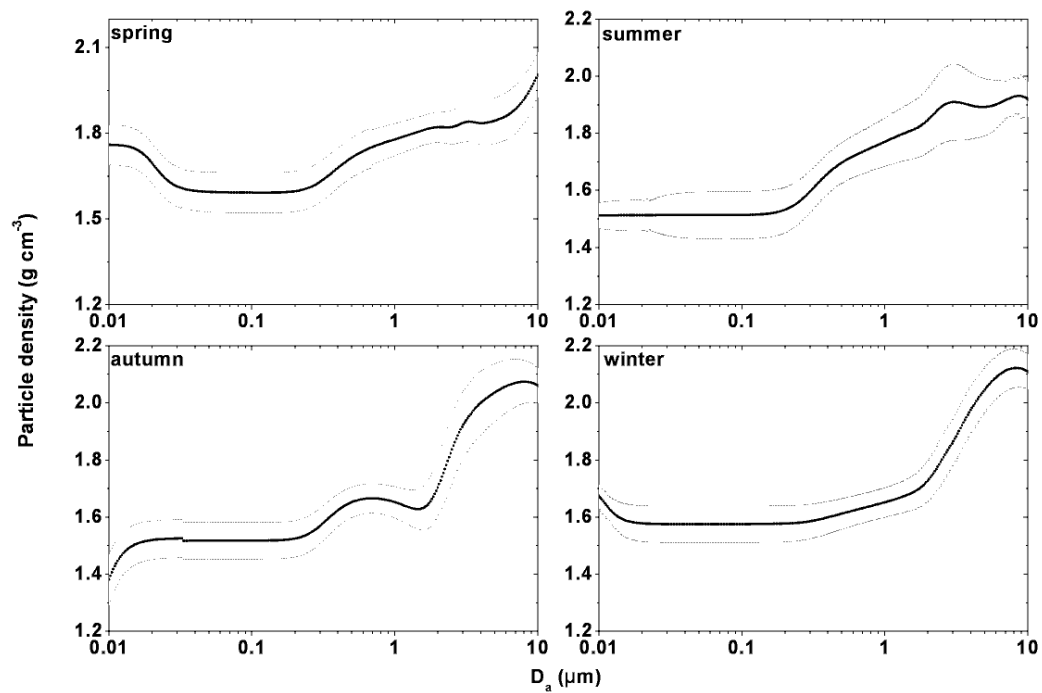


Figure S4. Continuous log-normal size distributions of seasonal average densities in four seasons.

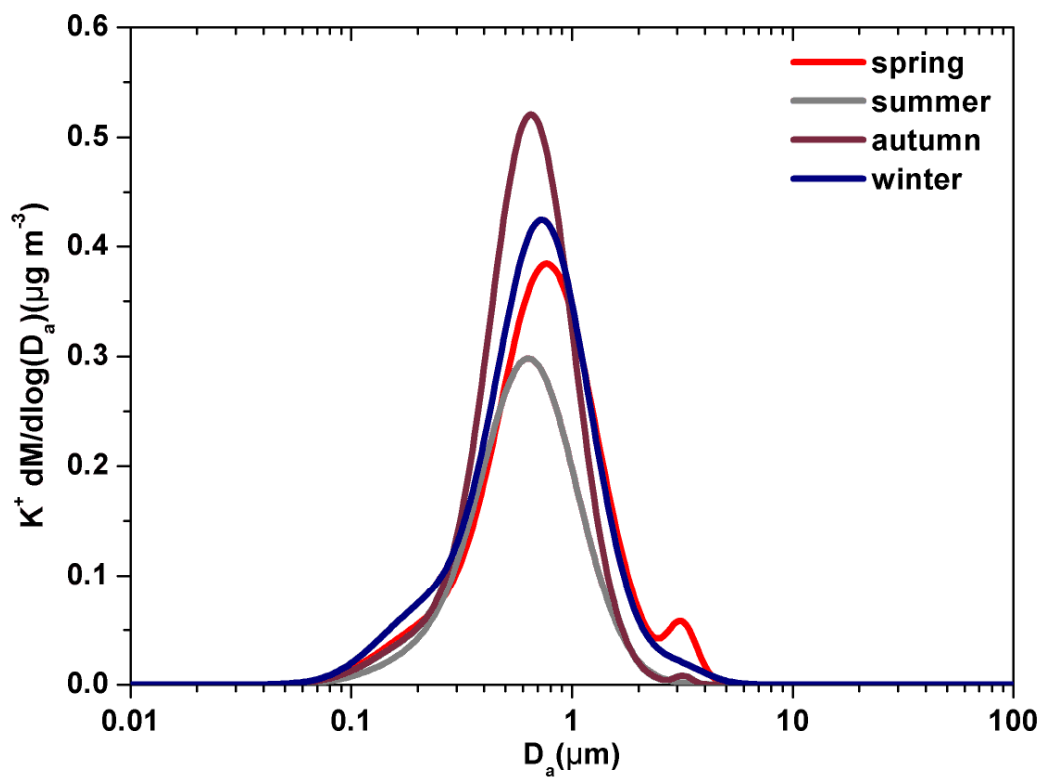


Figure S5. Continuous log-normal size distributions of K^+ in four seasons.

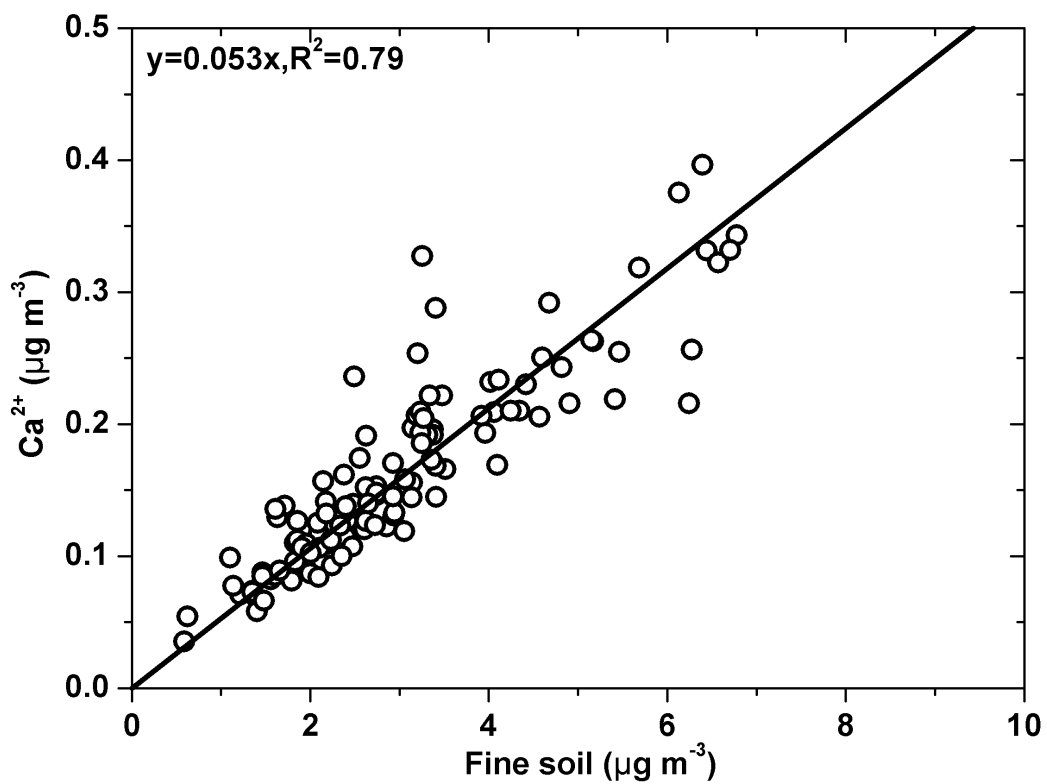


Figure S6. Correlations between Ca^{2+} and fine soil concentrations ($2.20[\text{Al}]+2.49[\text{Si}]+1.63[\text{Ca}]+2.42[\text{Fe}]+1.94[\text{Ti}]$) in four seasons in Guangzhou during 2014.

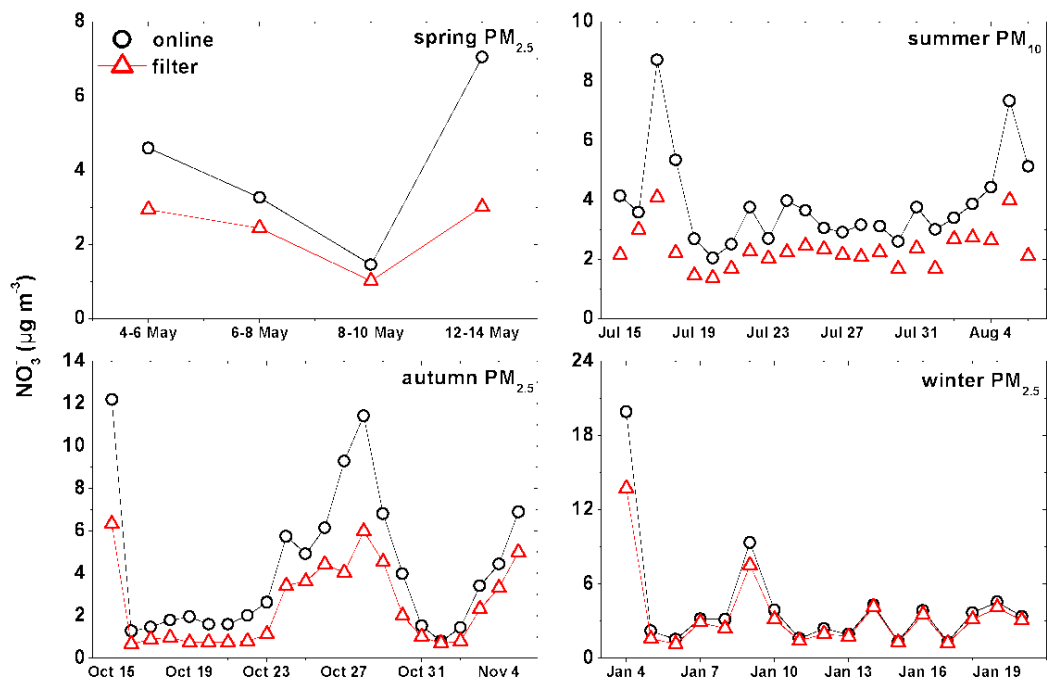


Figure S7. Correlations between filter-base and online NO_3^- concentrations in four seasons in Guangzhou.

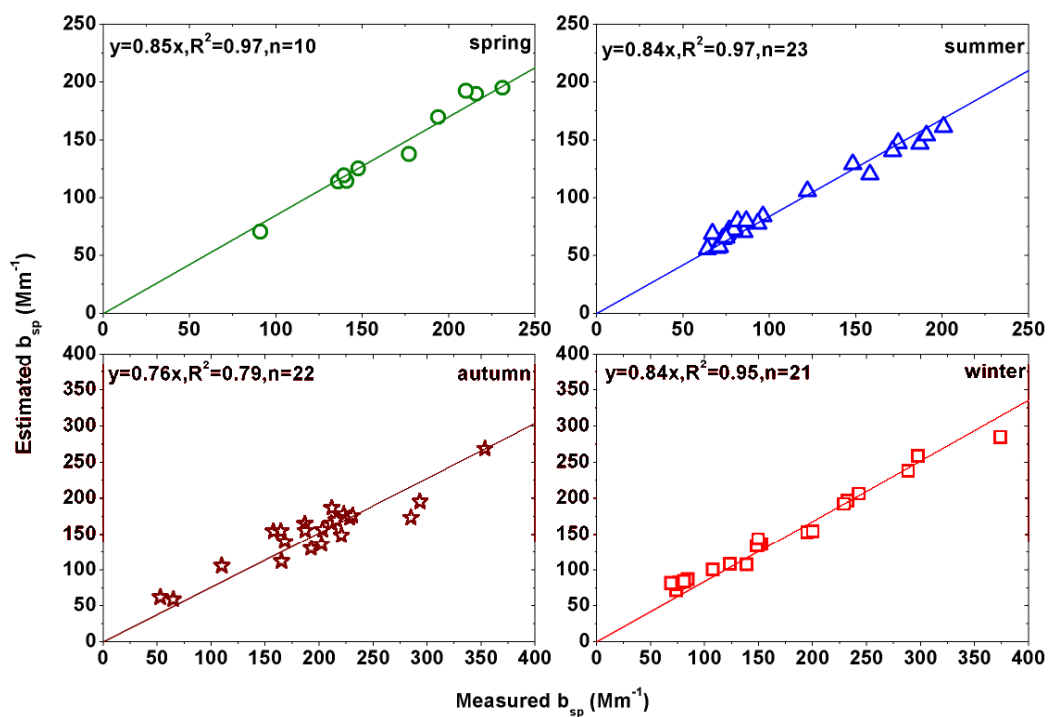


Figure S8. Correlations between the measured b_{sp} ($<100 \mu m$) at wavelength of 520 nm under dry condition (relative humidity $<30\%$) and estimated b_{sp} ($<10 \mu m$) using average MSEs of chemical species at wavelength of 550 nm under dry condition (relative humidity $=40\%$) in four seasons.